arXiv:1510.04170v2 [gr-qc] 16 Mar 2016

Imaging a boson star at the Galactic center

F H Vincent[1,2], Z Meliani[3], P. Grandclément[3], E. Gourgoulhon[3], O Straub[3]

[1] LESIA, Observatoire de Paris, PSL Research University, CNRS UMR 8109, Université Pierre et Marie Curie, Université Paris Diderot, 5 place Jules Janssen, 92190 Meudon, France

[2] Nicolaus Copernicus Astronomical Center, ul. Bartycka 18, PL-00-716 Warszawa, Poland

[3] LUTH, Observatoire de Paris, PSL Research University, CNRS UMR 8102, Universite Paris Diderot, 5 place Jules Janssen, 92190 Meudon Cedex, France

E-mail: `frederic.vincent@obspm.fr`

Abstract.

Millimeter very long baseline interferometry will soon produce accurate images of the closest surroundings of the supermassive compact object at the center of the Galaxy, Sgr A*. These images may reveal the existence of a central faint region, the so-called shadow, which is often interpreted as the observable consequence of the event horizon of a black hole. In this paper, we compute images of an accretion torus around Sgr A* assuming this compact object is a boson star, i.e. an alternative to black holes within general relativity, with no event horizon and no hard surface. We show that very relativistic rotating boson stars produce images extremely similar to Kerr black holes, showing in particular shadow-like and photon-ring-like structures. This result highlights the extreme difficulty of unambiguously telling the existence of an event horizon from strong-field images.

1. Introduction

Kerr black holes are characterized by the existence of an event horizon, a surface that separates the innermost region of spacetime from which no photons can reach a distant observer. The image of the vicinity of a Kerr black hole surrounded by an optically thin accretion flow is characterized by two specific features. The central part of the image is dark because the black hole has by definition no emitting surface and its event horizon captures photons traveling in the most central parts of the spacetime. This dark central area is known as the black hole *shadow* (Falcke et al. 2000)‡. This shadow is surrounded by a bright ring, the so-called *photon ring*, made of photons winding for one or many orbits in the very strong-field region extremely close to the black hole's event horizon.

‡ The term *silhouette* is often used in place of shadow. We keep here the original word, which describes properly the central fuzzy dark region of strong-field images.

The shape and angular size of the photon ring (or, equivalently, that of the shadow) contains very important information on the spacetime geometry because it depends on the properties of the compact object. For a Kerr black hole, the shadow slightly changes with the observer's inclination angle and with the black hole spin parameter (Johannsen 2013). Many articles have investigated whether alternative compact objects exhibit differences with respect to Kerr predictions (Bambi & Freese 2009; Johannsen & Psaltis 2010; Amarilla et al. 2010; Amarilla & Eiroa 2013; Vincent 2014; Moffat 2015; Cunha et al. 2015).

These two specific features of the Kerr black hole, the shadow and the photon ring, have attracted considerable attention in the last few years because of the development of millimeter Very Long Baseline Interferometry (VLBI). In particular, the *Event Horizon Telescope* (EHT, Doeleman et al. 2009), which will become fully operational around 2020, will reach an angular resolution of ≈ 20 μas. This is less than the angular size of the shadow of the central black hole in our Galaxy, Sgr A*, which is ≈ 50 μas, varying only slightly with the black hole spin. We note that the first EHT data were able to constrain the intrinsic angular size of the emitting region close to Sgr A* to only 37 μas (Doeleman et al. 2008). The shadow of the central black hole of the galaxy M87 has an angular size of roughly half the size of Sgr A* and is also a target of the EHT. As a consequence, very near-future observations might allow constraining the Kerr metric parameters and in particular the black hole spin from observing the size of the shadow of Sgr A* and M87. It might even be possible to constrain the actual theory of gravity in case the observed shadow cannot be fitted by using the Kerr metric.

The capability of VLBI to demonstrate the existence of a shadow at Sgr A* was first advocated by Falcke et al. (2000). This reference put forward the fact that detecting a shadow would be a proof of the existence of an event horizon. Since then many articles have been investigating shadows and photon rings in the perspective of the EHT (see the references given above). These works are generally following one of three ways. They consider the observable predictions of strong-field images:

- either of a specific alternative theory of gravity,
- or of some specific alternative compact object within general relativity,
- or of some parameterization of the non-Kerrness of spacetime.

The last way will probably be the most efficient when analyzing an important set of data will be at stake. However the two first ones are very important as well in order to determine how specific to the Kerr metric the EHT observables are and in particular the existence and angular size of the black hole shadow and photon ring.

This paper aims at developing the second way put forward above. We are interested in determining the observable predictions of strong-field images of accretion flows around *boson stars* (Feinblum & McKinley 1968; Kaup 1968; Ruffini & Bonazzola 1969). These are alternative compact objects within the classical theory of general relativity. Boson stars are particularly interesting as far as the future EHT data are concerned because these objects have *no event horizon and no emitting hard surface*. They are thus perfect

testbeds for examining whether shadows are indeed a probe of the existence of an event horizon and for determining the potential changes of a strong-field image caused by the absence of such an event horizon, but still without any emitting hard surface (which is an important difference with respect to an other well-studied alternative to black holes, the gravastar, Mazur & Mottola 2004). This paper focuses on the particular case of the accretion flow surrounding Sgr A* as we have been investigating this environment in a recent work (Vincent et al. 2015).

This work is one step in a series of paper aiming at examining the physical and astrophysical properties of boson stars (Grandclément et al. 2014; Meliani et al. 2015).

Section 2 presents boson stars and the accretion structure we consider. Section 3 gives our main results consisting in images and spectra of accretion tori surrounding boson stars. Section 4 provides conclusions.

2. Boson stars and accretion tori at Sgr A*

2.1. Boson stars

Boson stars are localized stable bundles of energy in the form of an assembly of spin-0 bosons. The idea of a soliton-like distribution of energy kept together by their own gravitational field dates back to the mid-50s with the so-called geons (a particle-like solution of the coupled field equations of general relativity and electromagnetism) developed by J. A. Wheeler (Wheeler 1955). What is now called a boson star was developed by Feinblum & McKinley (1968); Kaup (1968); Ruffini & Bonazzola (1969) who considered the Einstein-Klein-Gordon set of equations describing the gravitational field created by an assembly of spin-0 bosons. Such boson stars are macroscopic quantum objects subject to the Heisenberg uncertainty principle. It is this principle that is at the basis of the fact that boson stars may not undergo complete gravitational collapse to form a black hole. A lot of work has been devoted to these objects and to their stability and we redirect to reviews containing the relevant references (Jetzer 1992; Schunck & Mielke 2003; Liebling & Palenzuela 2012).

As of today, the only fundamental spin-0 boson is the Higgs boson detected recently by the Large Hadron Collider. Should boson stars be made of Higgs bosons, we would have to assume that the physical conditions inside these objects make it possible for the Higgs decay processes and their reverse to reach an equilibrium, in much the same way as for the β decay in neutron stars.

A boson star is described by the Lagrangian

$$L_{\rm BS} = L_g + L_\Phi \tag{1}$$

where L_g is the Lagrangian of the gravitation field and L_Φ is the Lagrangian of a massive complex scalar field. Boson stars are objects described in the framework of classical general relativity with minimal coupling of the scalar field. Accordingly

$$L_g = L_{\rm EH} = \frac{1}{16\pi G} R \tag{2}$$

is the standard Einstein-Hilbert Lagrangian, R being the Ricci scalar. The Lagrangian of the scalar field reads

$$L_\Phi = -\frac{1}{2}\left(\nabla_\mu \Phi \nabla^\mu \bar{\Phi} + \frac{m^2}{\hbar^2}|\Phi|^2\right) \tag{3}$$

where Φ is the complex scalar field. Boson stars are constructed by demanding it takes the form

$$\Phi = \phi(r,\theta) \times \exp\left(i(\omega t - k\varphi)\right) \tag{4}$$

where ϕ being its modulus, ω its frequency and the integer k its azimuthal number. Throughout this paper, unless otherwise stated, we use quasi-isotropic coordinates (t, r, θ, φ). Note that although the scalar field is time-dependent, the spacetime metric of boson stars is stationary. This is allowed by the simple harmonic time dependence of the scalar field and by the fact that its energy-momentum tensor only depends on the modulus of Φ.

The parameter m is the mass of one individual boson which should not be confused with the total mass of the boson star. In this framework, a boson-star spacetime is fully described by two parameters, the frequency ω and the azimuthal number k. The boson mass m is simply a scaling parameter, in much the same way as the Kerr black hole mass. It can be shown that the pair (ω, k) should satisfy (Grandclément et al. 2014)

$$\begin{aligned} &0 < \omega \leq \frac{m}{\hbar}, \\ &k \in \mathbb{N}. \end{aligned} \tag{5}$$

The closer ω is to $m/\hbar$, the less relativistic (i.e. compact) is the boson star (Grandclément et al. 2014). At the limit of $\omega \to m/\hbar$, the scalar field vanishes. The boson star's angular momentum is directly proportional to the azimuthal number (Schunck & Mielke 1998; Grandclément et al. 2014)

$$J = k\hbar\mathcal{N} \tag{6}$$

where $\mathcal{N}$ is the total particle number of the boson star. Thus the angular momentum is simply proportional to k. It is straightforward to compute a dimensionless spin parameter for a boson star in exactly the same way as for a Kerr black hole§

$$a = \frac{J}{M^2} \tag{7}$$

where M is the total ADM (Arnowitt, Deser, Misner) mass of the boson star. It is to be noted that contrarily to the Kerr black hole case, a is not restricted to be smaller than 1 (Ryan 1997; Grandclément et al. 2014; Meliani et al. 2015). In the Kerr case, the horizon is no longer defined for $a > 1$ and the central singularity becomes naked. As there is no event horizon nor a singularity for a boson star, nothing particular occurs when $a > 1$.

§ The Kerr spin parameter is $a = J/M$ and has the dimension of M. In this article we will consider the dimensionless quantity $a = J/M^2$ and call it spin for simplicity.

We have not considered any self-interaction potential between the bosons, meaning that our study is restricted to the so-called mini boson stars. We note that this restriction to mini boson stars is important as far as astrophysical applications are concerned because the maximum mass of a boson star is strongly dependent on the existence or non-existence of interactions between bosons (Colpi et al. 1986). For a mini boson star with an azimuthal number of order a few, the total mass M satisfies (Grandclément et al. 2014)

$$M < M_{\rm max} = \alpha \frac{m_p^2}{m} \tag{8}$$

where α is a coefficient of order $1-10$ and m_p is the Planck mass. For a Higgs boson ($m = 125$ GeV), the maximum mass is of order $10^{-21}\,M_\odot$, which is of course unable to account for any black-hole-like astrophysical source. In order to get a total mass of $\approx 10^6\,M_\odot$ (of the order of the mass of Sgr A*), the individual bosons should have a mass of 10^{-16} eV. We note again that much higher masses (consistent with supermassive black holes) can be produced by taking self-interaction into account, without having to postulate the existence of extremely light bosons (Colpi et al. 1986). However, for the sake of simplicity, we do not consider such an interaction in this paper. We thus assume the existence of very light spin-0 bosons in order to model Sgr A* by a mini boson star. We also note that Amaro-Seoane et al. (2010) has provided limits on m based on dark matter models, which are not compatible with the very small value assumed here. However, we do not try in this paper to model self-consistently supermassive black holes and dark matter with the same scalar field.

It is not obvious to model black hole candidates of very different masses with the same boson. Once the parameter m is fixed, the total mass of the boson star is restricted between 0 and the maximum mass $M_{\rm max}$ introduced above. As a consequence it may seem that if a boson light enough to model the most massive supermassive black holes was existing, it would be possible to model with the same boson all black hole candidates, whatever their mass (from stellar-mass to supermassive). However, this is not obvious because the total mass of the boson star can become very small with respect to m_p^2/m only in the limit of $\omega \to m/\hbar$. And as ω grows towards this limit, the distribution of the scalar field becomes less and less compact and the spacetime becomes less and less relativistic (Grandclément et al. 2014). As a consequence it appears difficult to model all black hole candidates with one common scalar field. It would probably be even problematic to model all supermassive black hole candidates (with masses from $\approx 10^6\,M_\odot$ to $\approx 10^{10}\,M_\odot$) with one common boson given the large mass span. However, it is not very likely that all black hole candidates in the Universe would be boson stars, it is very possible that Kerr black holes would coexist with boson stars. In this article, we will not investigate this question any further and we only consider one object, Sgr A*, for which we chose the boson mass m.

Varying the action constructed from the Lagrangian $L_{\rm BS}$ with respect to the metric leads to the usual Einstein field equations with the energy-momentum tensor of the scalar field. Varying it with respect to the scalar field leads to Klein-Gordon equation. This set

of equations is solved using the KADATH library (Grandclément 2010; Grandclément et al. 2014). In this paper, we use the set of metrics derived in Grandclément et al. (2014). We will consider only a few pairs of (k, ω) corresponding to few of the solutions illustrated in Figure 6 of Grandclément et al. (2014) and referenced in Table 2. In particular, we will not consider any boson-star spacetime containing an ergoregion as these solutions are unstable (Friedman 1978). However, the timescale of the instability is not known and may be high enough to allow such configurations to exist (Grandclément et al. 2014). We will consider rotating boson stars with azimuthal number $k = 1$ and $k = 4$, corresponding to the smallest and highest angular momentum of rotating boson stars computed in Grandclément et al. (2014). We will consider three values of the frequency, $\omega = 0.7, 0.8, 0.9\, m/\hbar$ spanning the spectrum from very relativistic ($\omega = 0.7\, m/\hbar$) to mildly relativistic ($\omega = 0.9\, m/\hbar$) solutions. For both $k = 1$ and $k = 4$, an ergoregion starts to develop for values of $\omega \lesssim 0.65\, m/\hbar$. We consider also non-rotating boson stars with $k = 0$, taking into account two values of the frequency $\omega = 0.83, 0.9\, m/\hbar$. For smaller values of the frequency, two solutions exist for the same value of ω (Grandclément et al. 2014) and we restrict ourselves to the region of the parameter space with only one solution for one pair (k, ω).

We note that two of these spacetimes are secularly unstable. Indeed, a curve $M(\omega)$ can be plotted for all values of k (see Fig. 6 of Grandclément et al. 2014). At least for the smallest values of k, this curve shows a maximum for some value $\omega_{\max}(k)$. A secular stability condition of the boson star is that $\omega > \omega_{\max}(k)$ (Friedman et al. 1988). As $\omega_{\max}(k = 4)$ is within the region of the $M(\omega)$ curve where an ergoregion exists, the $k = 4$ spacetimes considered here are all stable. However, $\omega_{\max}(k = 0) \approx 0.86$ and $\omega_{\max}(k = 1) \approx 0.77$, thus the $(k = 0, \omega = 0.83)$ and $(k = 1, \omega = 0.7)$ spacetimes are secularly unstable. We are still interested to investigate them in order to obtain a broad range of boson-star images, with also very relativistic configurations (i.e. with small values of frequency).

2.2. Accretion tori

The dynamical evolution of normal (baryonic) matter accreted onto a boson star has not been much investigated in the past. Torres (2002) dating back to more than 10 years ago seems to still contain the most developed discussion. It considers one of the most important questions, which is the possibility that accreting matter, by concentrating to the center of the boson star, would create a black hole there that could grow and ultimately encompass most of the scalar field distribution below its horizon. Considering this problem, Torres (2002) shows that if a supermassive boson star is present at the Galactic center and accretes at the current rate during the age of the Universe, it would still be 2 orders of magnitude less massive than Sgr A* (note that this computation is using a very high value of the accretion rate in the innermost accretion flow - $10^{-6}\, M_\odot\, \mathrm{yr}^{-1}$- so it should be considered as an upper limit). This is an argument in favor of the fact that should a supermassive boson star exist at Sgr A*, it

could not have been turned into a black hole by accreting normal matter to its center. We also note that it is not straightforward that matter would be able to accumulate at the center of the boson star: it should in particular be able to fight against a strong angular momentum barrier. Moreover, Torres et al. (2000) advocates the idea that stars accreted by a boson star at the Galactic center would be fully disrupted by tidal effects and that the remaining matter would end in unbound orbits, thus not accumulating at the center. However, more work is needed in this area to get a clear picture of how accreted matter would behave and how likely it is to form a black hole at the center of an accreting boson star. In this article, we consider a stationary toroidal accretion configuration and we do not discuss its stability.

We model the accretion flow surrounding Sgr A* by a constant-specific-angular-momentum, circularly-orbiting, perfect-fluid, polytropic accretion torus. We have already studied the properties of such accretion tori surrounding boson stars (Meliani et al. 2015). We combine here this work with our recent model of an accretion torus surrounding a Kerr black hole at Sgr A* (Vincent et al. 2015). Exactly the same model is used here, meaning that millimeter synchrotron radiation is emitted by the optically thin accretion torus. We refer to Vincent et al. (2015) for more details. The main difference between the Kerr case and the boson star case, as far as accretion tori are concerned, is that there does not always exist a self-crossing equi-pressure line (a cusp) in a boson-star spacetime (Meliani et al. 2015). In Vincent et al. (2015) we assumed that the inner radius of the torus is located at the cusp (which always exists for a Kerr black hole). In a boson star spacetime, we choose rather to let the inner radius be a free parameter. As a consequence, an accretion torus surrounding a boson star is described by 9 parameters (referenced in Tables 1 and 2): the boson-star parameters (ω, k), the observer's inclination i, the constant angular momentum $\ell = -u_\varphi/u_t$ (where $\mathbf{u}$ is the fluid 4-velocity), the polytropic index k_p, the inner radius of the torus r_in, the torus central temperature T_c and number density n_c, and the plasma β parameter being the ratio of the gas to magnetic pressures.

3. Images and spectra

In the whole paper, images and spectra of accretion tori surrounding black holes and boson stars are computed using the open-source‖ GYOTO code (Vincent et al. 2011). Photons are traced backwards in time from a distant observer by integrating the geodesic equation using a Runge-Kutta-Fehlberg adaptive-step integrator at order 7/8 (meaning that the method is 8th order, with an error estimation at 7th order). The integration is performed in the Kerr metric (Section 3.1) or in the numerical spacetime of a boson star computed by the KADATH library (Section 3.2). The equation of radiative transfer is integrated inside the optically thin torus to determine the value of specific intensity reaching the observer in each direction on sky (i.e. in each pixel of the observer's screen).

‖ Freely available at `http://gyoto.obspm.fr`

3.1. Accretion tori around a Kerr black hole

3.1.1. Reference Kerr image This section is meant to define a "reference" image of an accretion torus surrounding a Kerr black hole, which will be used to interpret the subsequent boson-star images. This setup is not the result of a proper fit, it is only a set of parameters which allows to reasonably account for the observable constraints that we currently have on the angular size of the emitting region at $\lambda = 1.3$ mm and on the millimeter spectrum of Sgr A*.

Typical spin parameters of boson stars are close to 1. The slowest-rotating (k=1) boson stars that we analyze here have spin parameters of order $a \approx 0.9$ (Meliani et al. 2015). As a consequence, we consider a Kerr spacetime with spin parameter $a = 0.9$. Table 1 shows the list of parameters which allows to get a reasonable fit in the Kerr spacetime. It leads to the 1.3 mm strong-field image and to the millimeter spectrum shown in Fig. 1. This Figure also shows the equi-pressure contours of the reference Kerr torus. We note in particular that the radial extent of the torus is of order $20\,M$.

We are interested in this paper in the modification of the strong-field image when the spacetime is changed. As a consequence, we will keep fixed to their Kerr values given in Table 1 all the astrophysical parameters $(\ell, n_c, T_c, k_{\rm p}, \beta)$ together with the inclination parameter i. The inner radius must be varied because different boson-star spacetimes lead to tori with different radial extension for the same value of $r_{\rm in}$, so that keeping the same value of $r_{\rm in}$ would have lead to very different looking images. We note that the total mass of the accretion torus is by many orders of magnitude smaller than the mass of Sgr A* which justifies the fact that we do not consider its contribution to the metric.

a	$\mathbf{i}$	$\boldsymbol{\ell}$	$r_{\rm in}$	$\mathbf{n_c}$	$\mathbf{T_c}$	$\mathbf{k_p}$	$\boldsymbol{\beta}$
0.9	85°	3.2 M	4.2 M	6.3×10^6 cm^{-3}	5.3×10^{10} K	5/3	10

Table 1. Parameters (introduced in Sect. 2.2) used to fit the spectral and imaging constraints in the Kerr spacetime. We remind that a is the dimensionless spin parameter, i is the observer's inclination angle, ℓ is the fluid angular momentum $-u_\varphi/u_t$, $r_{\rm in}$ is the torus inner radius, n_c and T_c are the torus central density and temperature, $k_{\rm p}$ is the polytropic index and β is the ratio of gas to magnetic pressures. Parameters in bold font will be kept fix in the whole paper. Only the spin parameter and the inner torus radius will vary.

At 1.3 mm, interstellar scattering is still important (Bower et al. 2006) and will degrade the image with respect to what is shown in Figure 1, essentially convolving it with a Gaussian of FWHM$\approx 20\,\mu$as. In this analysis, we assume that this effect can be fully corrected (see (Fish et al. 2014) for a recent discussion).

Figure 1 illustrates the notions of shadow and photon ring introduced earlier. The photon ring is the bright nearly circular ring of light at the center of the image. It is

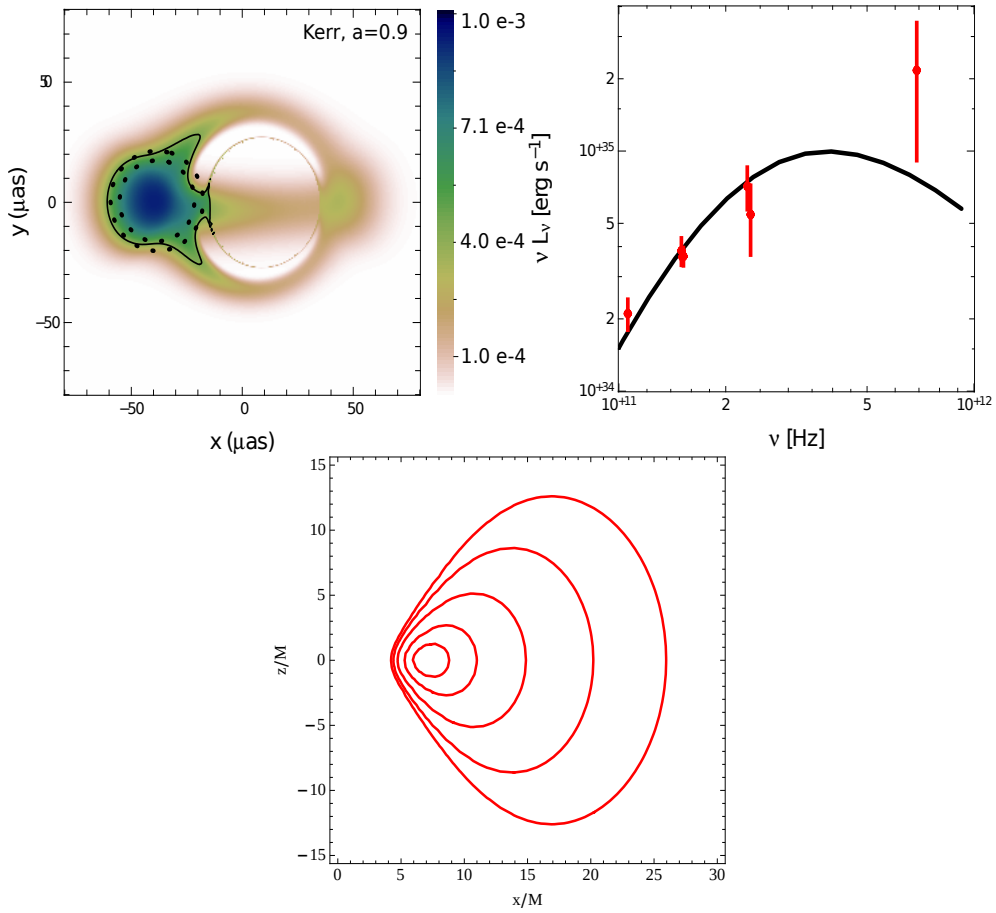

Figure 1. *The reference Kerr case.* **Upper left:** image at $\lambda = 1.3$ mm of an accretion torus surrounding a Kerr black hole with the parameters given in Table 1. The color bar indicates the cgs value of specific intensity. The dotted circles show the 1σ confidence limit for the intrinsic (no scattering included) angular size of the emitting zone (Doeleman et al. 2008). The solid black contour encompasses the region of the accretion flow emitting 50% of the total flux. **Upper right:** millimeter spectrum of the accretion torus, with red data points from (Falcke et al. 1998; Marrone et al. 2006). **Lower panel:** equi-pressure contours of the accretion torus in the (x, z) plane, z being along the rotation axis.

nearly exactly the outer limit of the black hole shadow, i.e. the locus of the directions on the observer's sky that asymptotically approach the event horizon when ray tracing backwards in time¶. Figure 2 gives a precise illustration of the location of the shadow. Comparing Figures 1 and 2 shows that the locus of the shadow is still illuminated in some parts because some radiation emitted by the accretion torus in between the compact object and the observer will fall inside the shadow when projected on sky. However, a strong gradient of specific intensity should be visible at least in some parts

¶ We note that geodesics ray traced backwards in time should never cross the event horizon as this would correspond to geodesics escaping the horizon, which is of course impossible. There is a stop condition in our ray-tracing code to prevent infinite integration when a photon approaches "too close" to the horizon.

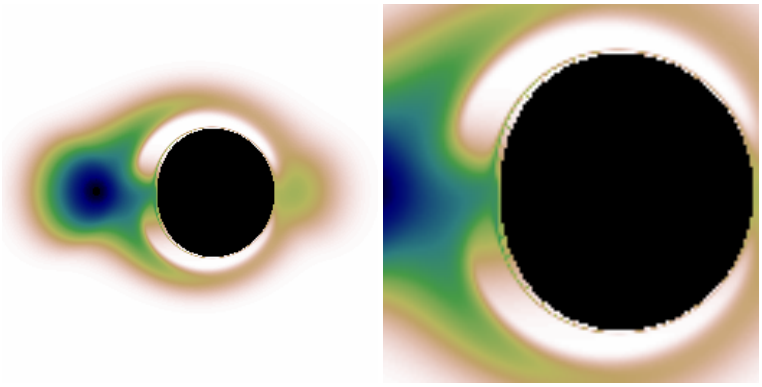

Figure 2. *Shadow and photon ring.* **Left:** same image as the left panel of Figure 1, but the directions on the observer's sky that asymptotically approach the event horizon when ray tracing backwards in time are marked in black color. The black area at the center of the image is the black hole shadow. Its exterior limit nearly coincides with the photon ring. **Right:** zoom on the central region.

of the photon ring (particularly away from the equatorial plane and from the part of the image boosted by the relativistic beaming effect, see Psaltis et al. 2014). In our model, matter is not emitting down to the event horizon: the inner edge of the torus ($r_{\rm in} = 4.2\,M$) is the closest region where radiation is emitted. This is a condition for getting such a clear photon ring as illustrated in Figure 1. However, even in case matter is emitting all the way down to the event horizon, there is still a sharp transition between the shadow and the outer region, as illustrated e.g. in Figure 1 of Falcke et al. (2000). As a consequence, it is really the strong gradient at the limit of the shadow which is the observable of interest, whatever the astrophysical model. Demonstrating the existence and measuring the angular size of this shadow (and of the surrounding photon ring if visible) is the main target of the EHT as far as strong-field gravity is concerned (see in particular Psaltis et al. 2014).

3.1.2. Ray tracing using an analytical or numerical Kerr metric Imaging boson stars will necessitate integrating geodesics in a numerical spacetime. In this section we compare the accuracy of two computations of the "reference" Kerr image. One image is integrated using the usual analytical expression of the Kerr metric in Boyer-Lindquist coordinates with a spin $a = 0.9$. The second image is integrated in a Kerr numerical spacetime (with $a = 0.9$ as well) computed using the LORENE library[+].This spacetime is described in quasi-isotropic coordinates which differ from Boyer-Lindquist coordinates and will be used to describe all boson-star spacetimes. Figure 3 shows the same strong-field image as already illustrated in the left panel of Figure 1 computed by the GYOTO code in both these spacetimes. These two images are indistinguishable by eye, and their respective fluxes differ by no more than 0.02% demonstrating that GYOTO is able to very accurately integrate geodesics in numerical spacetimes. We insist on

[+] Available at `http://www.lorene.obspm.fr`

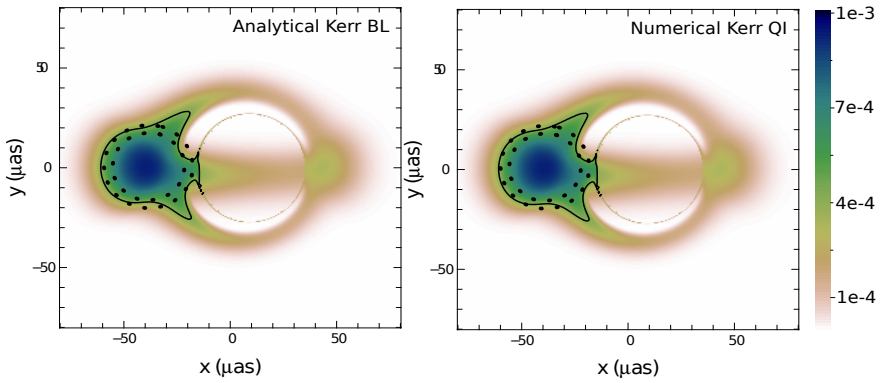

Figure 3. *Integration in numerical spacetimes.* **Left:** Kerr "reference" image described in Section 3.1.1 computed by the GYOTO code using the usual analytic Kerr metric with spin $a = 0.9$ in Boyer-Lindquist (BL) coordinates. **Right:** the same image computed by GYOTO using a numerical Kerr spacetime with the same spin, in quasi-isotropic (QI) coordinates. The two images have the same flux within a relative error of 0.02%.

the fact that the analytical and numerical spacetimes are described in very different coordinate systems (for instance the radial coordinate values at the horizon, $r_{\rm BL}$ and $r_{\rm QI}$ for Boyer-Lindquist and quasi-isotropic coordinates, differ by a factor ≈ 4.6) and that the observable, Figure 3, is the same as it should.

3.2. Accretion tori around a boson star

3.2.1. Tori setups Accretion tori surrounding boson stars can be computed relatively easily, in much the same way as in the more standard Kerr case. Our recent analysis (Meliani et al. 2015) highlights some of the main properties of these structures. In this section, we are interested in examining the modification on strong-field images imposed by the change of spacetime. As a consequence, we will keep fixed nearly all model parameters to the values given in Table 1. Fixing the inner radius fixes the radial extent of the torus in a given spacetime, but this radial extent depends quite strongly on the spacetime. Therefore, we do not decide to keep the inner radius fixed, but rather to choose the inner radius in order to get, for all spacetimes considered, a radial extent of roughly $20\,M$ in Boyer-Lindquist coordinates (which is the radial extent of the reference torus in the Kerr metric described in Section 3.1.1).

Table 2 gives the parameters used for all boson-star setups. All the parameters which are not mentioned have the same value as in Table 1. Note that the dimensionless spin parameter a can become bigger than 1 as opposed to the Kerr black hole case. There is nothing particular with a boson-star spacetime with a spin bigger than 1. In particular there is of course no naked singularity (as would be the case in the Kerr spacetime with $a > 1$).

Figure 4 shows the contours of the equi-pressure surfaces of these tori together with the contours of the scalar field modulus ϕ. These panels highlight the fact that when the

(k,ω)	M	a	$r_{\rm in}$
$(0, 0.83\,m/\hbar)$	$0.63\,\mathcal{M}$	0.00	$4.39\,M$
$(0, 0.9\,m/\hbar)$	$0.60\,\mathcal{M}$	0.00	$5.80\,M$
$(1, 0.7\,m/\hbar)$	$1.26\,\mathcal{M}$	0.82	$2.72\,M$
$(1, 0.8\,m/\hbar)$	$1.31\,\mathcal{M}$	0.80	$2.84\,M$
$(1, 0.9\,m/\hbar)$	$1.12\,\mathcal{M}$	0.92	$4.90\,M$
$(4, 0.7\,m/\hbar)$	$3.90\,\mathcal{M}$	1.13	$3.34\,M$
$(4, 0.8\,m/\hbar)$	$3.35\,\mathcal{M}$	1.27	$2.92\,M$
$(4, 0.9\,m/\hbar)$	$2.52\,\mathcal{M}$	1.64	$5.30\,M$

Table 2. *Parameters used to compute accretion tori in the various boson-star spacetimes considered here. M is the ADM mass given in units of $\mathcal{M} = m_p^2/m$.*

boson star is rotating, the scalar field distribution has a toroidal topology. The name boson "star" (suggestive of a spherical topology) is thus misleading for such objects, however we keep using it for historical reasons. While the contours of the torus remain rather similar for all spacetimes (including the Kerr spacetime, see the right panel of Figure 1), the scalar field distribution is a bit more peaked for higher rotation and much more peaked for more relativistic spacetimes. This will translate in more important lensing effects in the strong-field region for very relativistic boson stars. We note also that the accretion torus and the scalar field distribution overlap in regions where the scalar field is still far from 0 (i.e., rather close to the center of the distribution), which does not lead to any physical effect as we assume that there is no interaction between normal (baryonic) matter and the scalar field.

3.2.2. Images and spectra Figure 5 shows the 1.3 mm images of all the tori setups surrounding boson stars given in Table 2. For less-relativistic setups ($\omega = 0.9\,m/\hbar$), which are closer to empty space (remember that $\omega = m/\hbar$ corresponds to empty space, see Section 2.1), images show a smooth distribution of specific intensity for all values of k, with no strong gradient (no "hole" at the center of these images). This is close to the image one would get in a Newtonian spacetime of a thick torus seen edge-on. For all values of k also, a region with much lower intensity value (a "hole") appears in the image as ω decreases. For very relativistic spacetimes ($\omega = 0.7$) this "hole" is accompanied by a bow-shape structure, which is the equivalent of the Kerr photon ring.

In order to understand these transitions, Figure 6 (top row) shows again the torus pressure and scalar field contours for $k = 1$ spacetimes, together with 3 geodesics projected in the $(x = r\sin\theta, z = r\cos\theta)$ plane. These panels show the increasing gravitational lensing effects on null geodesics as ω decreases and the spacetime becomes more relativistic. When the lensing effect is strong enough, a low-intensity region appears at the center of the images. When this effect is even stronger, two geodesics

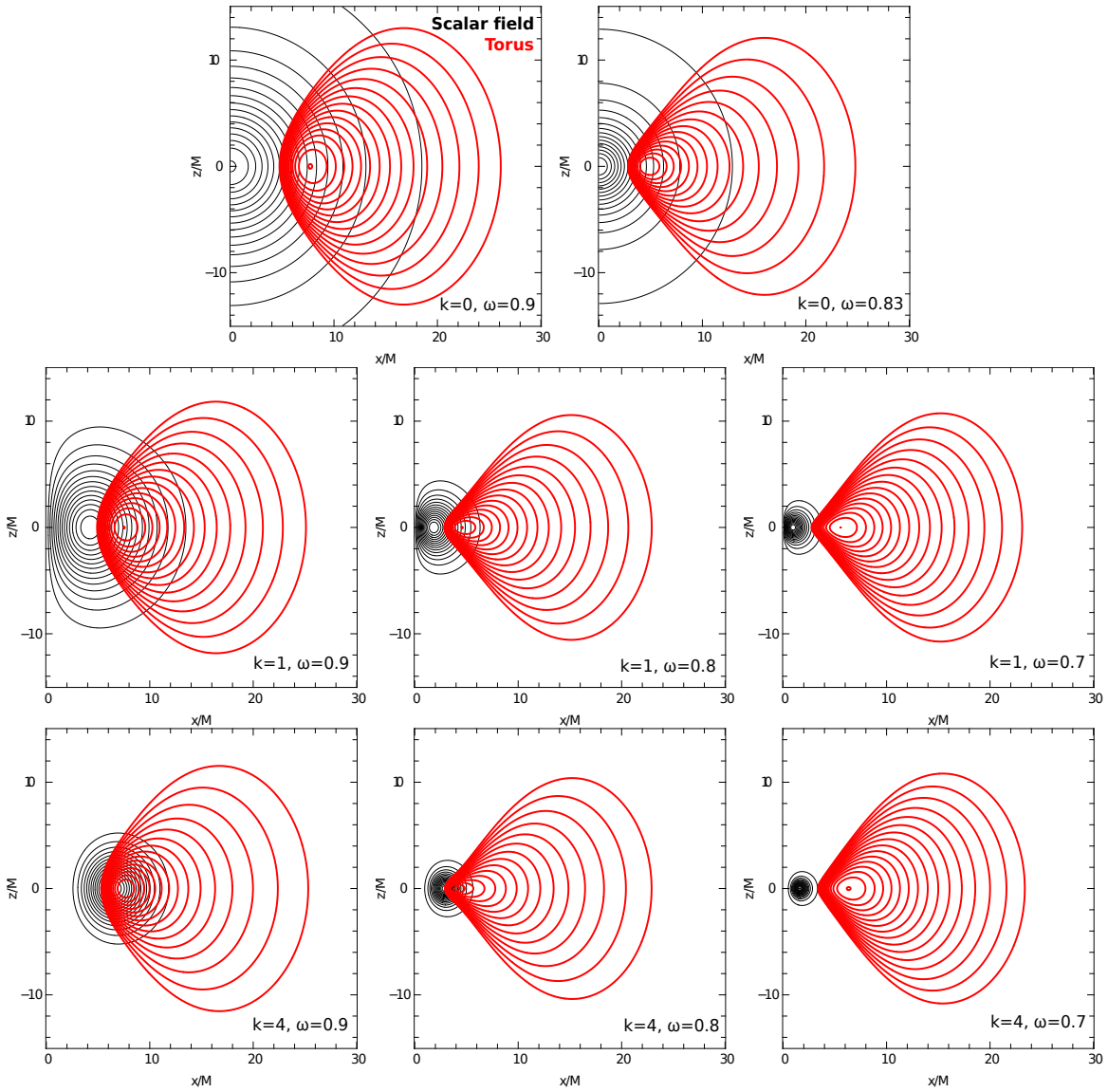

Figure 4. *Boson-star accretion tori contours.* Equi-pressure contours of the accretion torus (red) and contours of the scalar field distribution (black) for the various setups described in Table 2, in the (x, z) plane, where z is a coordinate along the rotation axis. The axes are labeled in units of the boson star total mass M. Boson star rotation is increasing from top to bottom (towards higher k), and the spacetime is more and more relativistic from left to right (towards smaller ω).

corresponding to very similar directions on sky (within $\approx 1\,\mu$as) can have very different trajectories, leading to the development of the bow-shape structure. The bottom panel of Figure 6 shows that this is similar to what causes the appearance of the Kerr photon ring. This bow-shape structure characteristic of very relativistic boson stars was first highlighted very recently by Cunha et al. (2015). Their Figure 4, middle-right panel shows an extremely similar structure to our $k = 1$, $\omega = 0.7$ image. This structure has a very comparable angular size to that of the reference Kerr photon ring. The most distant part of the Kerr photon ring from the center of coordinates (to the right of the

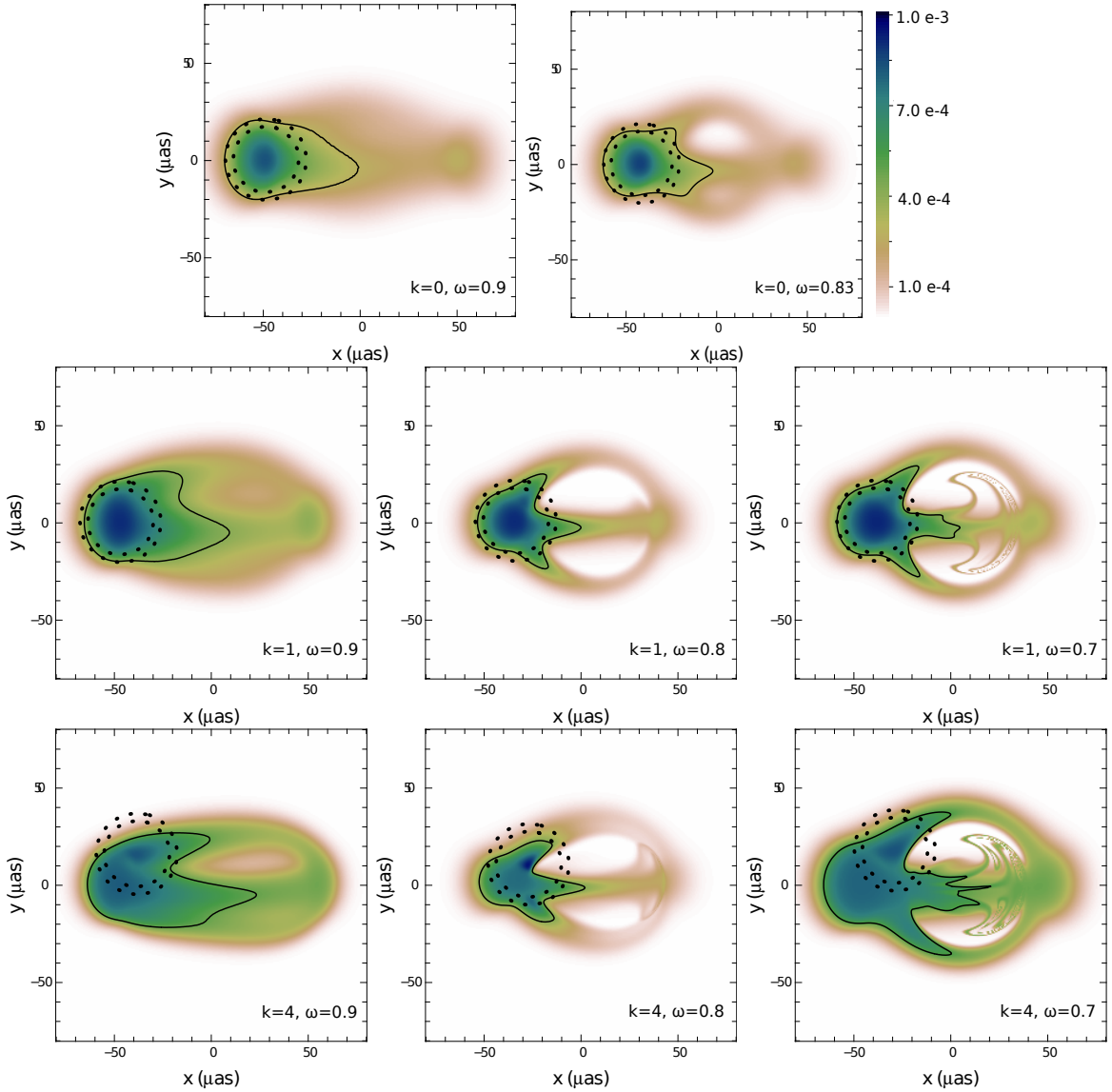

Figure 5. *Boson-star images.* Maps of specific intensity distribution for the various boson-star setups given in Table 2. The color bar at the top right is valid for all panels and is graduated in cgs units. The dotted circles show the 1σ confidence limit on the angular size of the emitting region imposed by the first VLBI measurements (Doeleman et al. 2008). They are centered on the maximum of the intensity distribution. The solid black contour encompasses the region emitting 50% of the total flux. The axes are labeled in μas, as measured on the distant observer's screen. Boson star rotation is increasing from top to bottom (towards higher k), and the spacetime is more and more relativistic from left to right (towards smaller ω).

image) is located at $\approx 35.5\,\mu$as while the most distant part of the bow-shape structure for the $(k = 1, \omega = 0.7\,m/\hbar)$ spacetime is located at $\approx 34.5\,\mu$as from the center of coordinates.

The superposition of the low-flux central region and of this bow-shape structure is extremely similar to the shadow+photon ring familiar structure in the Kerr spacetime. In particular, it shows that detecting a shadow (i.e. a low-flux region surounded by a bright portion of arc) is not sufficient to tell the existence of an event horizon, as suggested by Falcke et al. (2000). It is probable that after distortion by the instrument's response function, it would be impossible to differentiate a Kerr image from a very relativistic boson-star image.

We note here a particularity of the $k = 4$ images. All other spacetimes give rise to an intensity distribution peaked more or less at the same point, to the left of the image in our geometry. This location corresponds to the maximum of the relativistic beaming effect due to the enhancement of radiation when the emitter is traveling towards the observer. However, the maximum of the intensity distribution is somewhat shifted with respect to this maximum beaming location for all $k = 4$ spacetimes. This is mainly due to the stronger bending of light rays as explained in Figure 7. This Figure compares the two geodesics corresponding to the location on sky of the intensity maxima of the $(k = 0, \omega = 0.9\,m/\hbar)$ and $(k = 4, \omega = 0.9\,m/\hbar)$ spacetimes. It shows that the geodesic corresponding to the maximum intensity location of the $(k = 4, \omega = 0.9\,m/\hbar)$ spacetime (dashed blue, right panel) visits the very central parts of the torus, which translates in a high intensity. On the contrary, the same geodesic in the $(k = 0, \omega = 0.9\,m/\hbar)$ spacetime (dashed blue, left panel) always stays rather far from the innermost torus regions. Strong light bending thus somewhat changes the flux distribution for $k = 4$ spacetimes.

Figure 8 shows the corresponding millimeter spectra for all boson-star spacetimes as well as for the Kerr reference case. It shows that different setups lead to different spectra. However, it is not likely that spectra can provide a way to differentiate alternative compact objects given how degenerate the different parameters are. Taking different values of the astrophysical parameters like the central density and temperature will lead to very different spectra while the angular size of the "shadow" (be it the usual Kerr shadow or the faint central region in highly relativistic boson-star spacetimes) will not differ as it is due to lensing effects which are independent of astrophysics. It is to be noticed still that the $(k = 1, \omega = 0.7\,m/\hbar)$ spectrum (dotted green) is extremely similar to the Kerr reference spectrum (solid black): both the image and the spectra are thus extremely similar to the Kerr case for this spacetime.

3.2.3. Photon orbit, bow-shape structure and spacetime stability The $(k = 1, \omega = 0.7)$ spacetime we highlighted in the previous Section as able to generate a Kerr-similar strong-field image may suffer from two stability issues.

First, this solution is located at $\omega < \omega_{\rm max}(k = 1)$ as already written in the Introduction. It is thus secularly unstable.

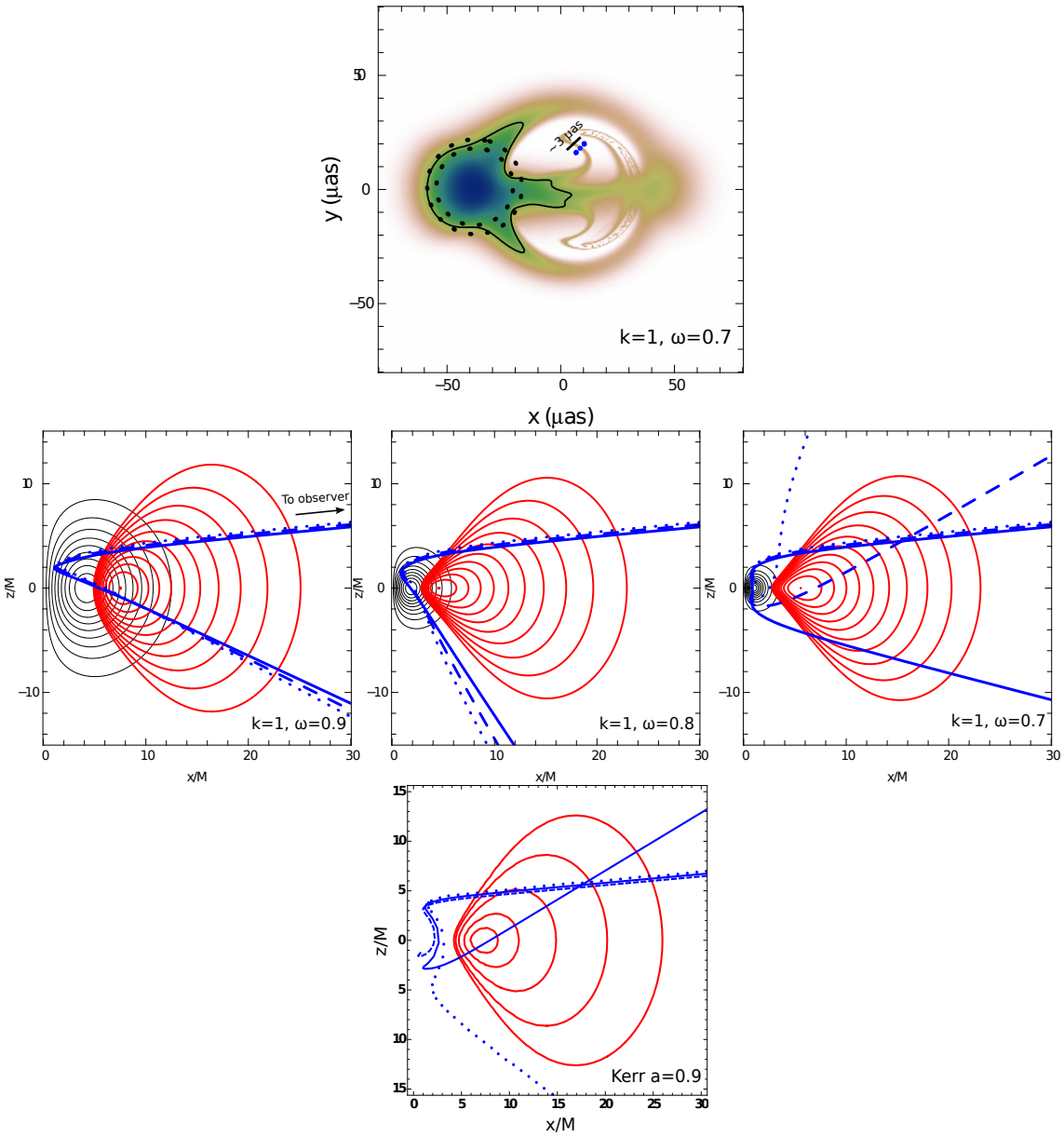

Figure 6. *Light bending.* **Top row**: the $k = 1$, $\omega = 0.7\,m/\hbar$ image with 3 blue dots corresponding to the directions on sky of the 3 geodesics represented in the middle row panels. These 3 directions are separated by only $\approx 3\,\mu$as. **Middle row:** same as Figure 4 for $k = 1$ boson stars, with 3 photon geodesics overplotted in blue in each panel, corresponding to the 3 directions on sky highlighted in the top panel. The geodesics are integrated backwards in time from the distant observer. They are computed in 3 space dimensions (r, θ, φ) and are projected here in $(x = r \sin\theta, z = r\cos\theta)$ whatever φ. Mind that part of the geodesics curvature on these plots is due to the projection from 3 to 2 space dimensions. The difference of magnitude of the lensing effect depending on the value of ω appears clearly. **Bottom row:** the same for the reference Kerr $a = 0.9$ case. The 3 geodesics represented here do not correspond to the same directions on sky as the previous ones. They are associated to the vicinity of the Kerr photon ring, i.e. to the most lensed geodesics in the Kerr spacetime. Note that the dashed geodesic asymptotically approaches the event horizon.

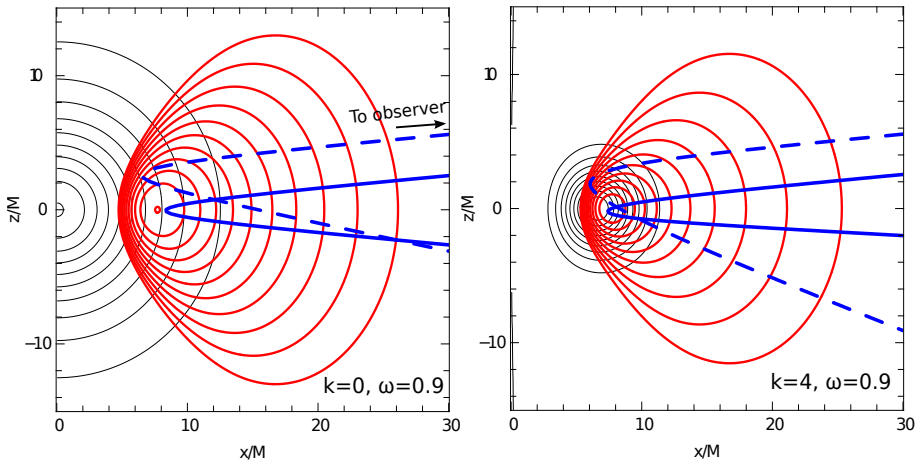

Figure 7. *Intensity maximum location.* Contours of the $\omega = 0.9\,m/\hbar$, $k = 0$ (left) and $k = 4$ (right) spacetimes. In blue, two geodesics are over-plotted. The solid one corresponds to the direction on the sky of the maximum of the intensity distribution of the $(k = 0, \omega = 0.9\,m/\hbar)$ setup (see Figure 5, upper left panel). The dashed one corresponds to the direction on the sky of the maximum of the intensity distribution of the $(k = 4, \omega = 0.9\,m/\hbar)$ setup (see Figure 5, lower left panel).

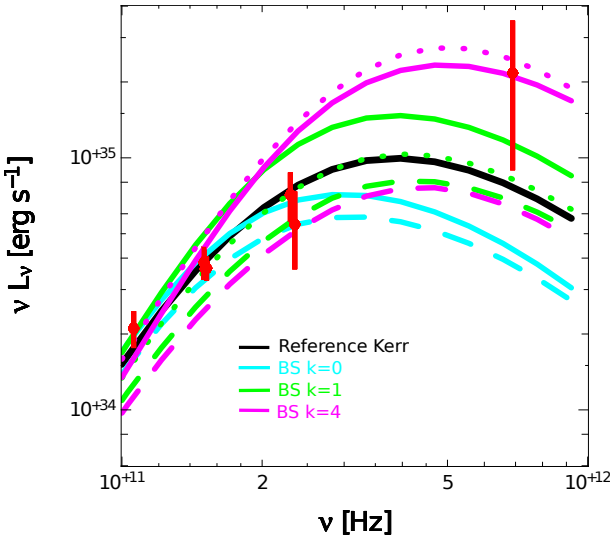

Figure 8. *Comparing millimeter spectra.* The Kerr reference spectrum is in solid black. Boson stars (BS) spectra are in cyan for $k = 0$, green for $k = 1$ and magenta for $k = 4$. Dotted lines are for $\omega = 0.7\,m/\hbar$, dashed lines for $\omega = 0.8\,m/\hbar$ and solid lines for $\omega = 0.9\,m/\hbar$ ($\omega = 0.83\,m/\hbar$ for the $k = 0$ case). We note the extreme similarity between the Kerr reference spectrum (solid black) and the $k = 1$, $\omega = 0.7\,m/\hbar$ boson-star spectrum (dotted green), corresponding to the very similar strong-field images shown in Figure 1, upper left panel, and Figure 5, middle right panel.

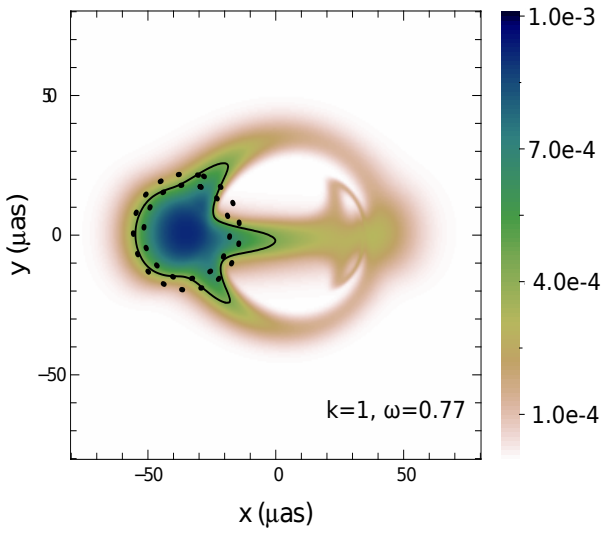

Figure 9. *Bow-shape structure for a spacetime with no stability issue.* Image at 1.3 mm for a $k = 1$, $\omega = 0.77$ boson star. This spacetime is most probably stable as it is on the stable branch of the $M(\omega)$ curve, has no photon orbit and no ergoregion. It still displays a bow-shape structure, although it is smaller than in Fig. 5, middle right panel.

Second, Cardoso et al. (2014) advocates the fact that all spacetimes with a stable photon orbit and no event horizon are unstable. The ($k = 1$, $\omega = 0.7$) spacetime indeed has a stable photon orbit. However, we believe that the statement of Cardoso et al. (2014) is not sufficient to be able to conclude with full confidence: a stability study of rotating boson-star spacetimes is thus very much needed.

Even if the ($k = 1, \omega = 0.7$) spacetime may not be astrophysically relevant, we consider that the fact that a spacetime with no event horizon can mimic a Kerr strong-field image is sufficiently interesting to be highlighted. However, in order to determine what the strong-field image will look like for a stable spacetime, we have computed one more image for $k = 1$ boson stars, considering a frequency of $\omega = 0.77$ (corresponding to the maximum of the $M(\omega)$ curve) which is secularly stable. Moreover, the ($k = 1$, $\omega = 0.77$) spacetime has no photon orbit and no ergoregion. There is thus to our knowledge no obvious reason to doubt its stability. The spin parameter of this configuration being $a = 0.8$, it is also compatible with a Kerr spacetime. Figure 9 shows a strong-field 1.3 mm image for this spacetime. It still displays the bow-shape structure typical of extremely strong lensing effect. This bow-shape structure, although smaller than in the ($k = 1$, $\omega = 0.7$) spacetime, is still similar to a portion of a Kerr photon ring. In particular, it appears on the Doppler deboosted part of the image, which is the primary target for detecting photon rings as highlighted by Psaltis et al. (2014).

Figure 9 thus shows that strong-field images with a clear decrease of intensity in the central parts (a "shadow") and strong gradients of intensity (the bow-shape structure, similar to a partly obscured photon ring) are not sufficient to tell an event horizon.

4. Conclusion

We have performed ray-tracing computations of accretion tori surrounding Kerr black holes and different kinds of boson stars in order to produce 1.3 mm images and spectra of the accretion flow surrounding Sgr A* in the perspective of future high-quality observations at this wavelength by the EHT. Our goal is to determine how strong-field images differ from the well-known Kerr case when considering boson stars, i.e. compact objects with no event horizon and no hard surface.

The main result of our research is Figure 5 and particularly its central right panel showing the image of an accretion torus around a $(k = 1, \omega = 0.7\, m/\hbar)$ boson star which is extremely similar to a Kerr strong-field image. In particular, the image shows a faint central region the angular size of which is very similar to that of the Kerr shadow for the same spin and orientation. This finding questions the assumption of Falcke et al. (2000) and many other authors that detecting a shadow (i.e. a faint central region separated by a strong intensity gradient from the exterior region) is a proof of the existence of an event horizon. Moreover, a bow-shape structure, due to very strong light bending close to the center of the scalar field distribution, is visible in highly relativistic boson-star spacetimes and is very similar to the Kerr photon ring.

Quite a few caveats should be noticed in order to interpret this result.

- A first obvious remark is that our model is stationary and made of a compact distribution of normal matter which is not extending down to $r = 0$ (which would be possible at least in theory for a boson-star spacetime given that there is no event horizon nor any singularity at $r = 0$). In case a long-lived accretion flow extending down to $r = 0$ and emitting sufficiently would be viable, it would not exhibit the same shadow-like central region. It is very difficult to predict what such a flow would look like and we are now developing general relativistic magnetohydrodynamics numerical simulations of such accretion structures in order to investigate this option.
- We are considering in this paper mini boson stars (with no self-interactions among bosons), meaning that we have to assume the existence of extremely light ($\approx 10^{-16}$ eV) spin-0 bosons in order to model Sgr A*. We plan to develop similar simulations as presented in this paper for self-interacting boson stars that would allow modeling supermassive compact objects with a much higher boson mass. We also note that Horvat et al. (2013) studied boson stars non-minimally coupled to gravity. This is another direction of generalization for the present work.
- Our model assumes the stability of an accretion flow made of normal matter and surrounding a boson star (for the typical parameters given in Table 2). We are not aware of any work studying in detail the evolution of baryonic matter around rotating boson stars, and in particular the possibility to form a black hole by accreting matter to $r = 0$. This is a very interesting area of research that we plan to investigate.
- Finally, we have been assuming that normal matter does not interact with bosons

except through gravitational interaction.

However, despite all these limiting remarks, we believe that our result highlights the extreme difficulty of interpreting strong-field images. In particular it shows the importance, for the future interpretation of EHT data, of studying the observable predictions of well-established alternative compact objects, in parallel to developing parameterized non-Kerr spacetimes. As highlighted by Cunha et al. (2015) it would be interesting to check whether these parameterized spacetimes can produce such structures as the bow-shape feature exhibited in Figure 5.

As a final remark, we would like to stress that the aim of this article is *not* to support the case for a boson star at the center of the Galaxy, or as an alternative to black hole candidates in general. Our aim is to investigate the simplest possible testbed of event-horizon-less spacetime. We believe that this simplest testbed is the boson-star model. As a consequence, boson stars are useful tools to investigate the power of experiments aiming at demonstrating the existence of black holes. Such experiments should first demonstrate their ability to tell a black hole from a boson star. This article shows that experiments based on the investigation of shadows of compact objects may not be valid tests of the existence of black holes because it is not clear that they are able to unambiguously differentiate a black hole from a boson star. It is possible, although not clear at the moment, that gravitational-wave tests could be a clean way to differentiate a black hole from a boson star (Ryan 1997; Kesden et al. 2005; Palenzuela et al. 2008).

Acknowledgments

FHV is grateful to Enrico Barausse for pointing out the work of Cardoso et al. (2014) and to Carlos Herdeiro, Helgi Runarsson and Thomas Sotiriou for stimulating discussions at a mini-workshop on scalar fields and gravitation in Meudon. FHV acknowledges financial support from the National Science Centre (NCN), Poland, grant 2013/09/B/ST9/00060 and was partially supported by the National Science Centre (NCN), Poland, DEC-2013/08/M/ST9/00664, within the framework of the HECOLS International Associated Laboratory. Part of this work was supported by the French PNHE (Programme National Hautes Énergies). ZM acknowledges financial support from the UnivEarthS Labex program at Sorbonne Paris Cité (ANR-10-LABX- 0023 and ANR-11-IDEX-0005-02). EG acknowledges support from the grant ANR-12-BS01-012-01 *Analyse Asymptotique en Relativité Générale*.

References

Amarilla, L. & Eiroa, E. F. 2013, Phys. Rev. D, 87, 044057

Amarilla, L., Eiroa, E. F., & Giribet, G. 2010, Phys. Rev. D, 81, 124045

Amaro-Seoane, P., Barranco, J., Bernal, A., & Rezzolla, L. 2010, J. Cosmology Astropart. Phys., 11, 2

Bambi, C. & Freese, K. 2009, Phys. Rev. D, 79, 043002

Bower, G. C., Goss, W. M., Falcke, H., Backer, D. C., & Lithwick, Y. 2006, ApJ, 648, L127

Cardoso, V., Crispino, L. C. B., Macedo, C. F. B., Okawa, H., & Pani, P. 2014, Phys. Rev. D, 90, 044069

Colpi, M., Shapiro, S. L., & Wasserman, I. 1986, Phys. Rev. Lett., 57, 2485

Cunha, P. V. P., Herdeiro, C. A. R., Radu, E., & Runarsson, H. F. 2015, ArXiv e-prints

Doeleman, S., Agol, E., Backer, D., et al. 2009, in Astronomy, Vol. 2010, astro2010: The Astronomy and Astrophysics Decadal Survey, 68

Doeleman, S. S., Weintroub, J., Rogers, A. E. E., et al. 2008, Nature, 455, 78

Falcke, H., Goss, W. M., Matsuo, H., et al. 1998, ApJ, 499, 731

Falcke, H., Melia, F., & Agol, E. 2000, ApJ, 528, L13

Feinblum, D. A. & McKinley, W. A. 1968, Phys. Rev., 168, 1445

Fish, V. L., Johnson, M. D., Lu, R.-S., et al. 2014, ApJ, 795, 134

Friedman, J. L. 1978, Communications in Mathematical Physics, 63, 243

Friedman, J. L., Ipser, J. R., & Sorkin, R. D. 1988, ApJ, 325, 722

Grandclément, P. 2010, Journal of Computational Physics, 229, 3334

Grandclément, P., Somé, C., & Gourgoulhon, E. 2014, Phys. Rev. D, 90, 024068

Horvat, D., Ilijić, S., Kirin, A., & Narančić, Z. 2013, Classical and Quantum Gravity, 30, 095014

Jetzer, P. 1992, Physics Reports, 220, 163

Johannsen, T. 2013, ApJ, 777, 170

Johannsen, T. & Psaltis, D. 2010, ApJ, 718, 446

Kaup, D. J. 1968, Phys. Rev., 172, 1331

Kesden, M., Gair, J., & Kamionkowski, M. 2005, Phys. Rev. D, 71, 044015

Liebling, S. L. & Palenzuela, C. 2012, Living Reviews in Relativity, 15, 6

Marrone, D. P., Moran, J. M., Zhao, J.-H., & Rao, R. 2006, Journal of Physics Conference Series, 54, 354

Mazur, P. O. & Mottola, E. 2004, Proceedings of the National Academy of Science, 101, 9545

Meliani, Z., Vincent, F. H., Grandclément, P., et al. 2015, Classical and Quantum Gravity, 32, 235022

Moffat, J. W. 2015, European Physical Journal C, 75, 130

Palenzuela, C., Lehner, L., & Liebling, S. L. 2008, Phys. Rev. D, 77, 044036

Psaltis, D., Ozel, F., Chan, C.-K., & Marrone, D. P. 2014, ArXiv e-prints

Ruffini, R. & Bonazzola, S. 1969, Phys. Rev., 187, 1767

Ryan, F. D. 1997, Phys. Rev. D, 55, 6081

Schunck, F. E. & Mielke, E. W. 1998, Physics Letters A, 249, 389

Schunck, F. E. & Mielke, E. W. 2003, Classical and Quantum Gravity, 20, R301

Torres, D. F. 2002, Nuclear Physics B, 626, 377

Torres, D. F., Capozziello, S., & Lambiase, G. 2000, Phys. Rev. D, 62, 104012

Vincent, F. H. 2014, Classical and Quantum Gravity, 31, 025010

Vincent, F. H., Paumard, T., Gourgoulhon, E., & Perrin, G. 2011, Classical and Quantum Gravity, 28, 225011

Vincent, F. H., Yan, W., Straub, O., Zdziarski, A. A., & Abramowicz, M. A. 2015, A&A, 574, A48

Wheeler, J. A. 1955, Phys. Rev., 97, 511